Experimental Thermal and Fluid Science 127 (2021) 110410

Contents lists available at ScienceDirect

Experimental Thermal and Fluid Science

journal homepage: www.elsevier.com/locate/etfs

An experimental study on the improvements in the film cooling performance by an upstream micro-vortex generator

Kuan Zheng [a], Wei Tian [a,*], Jiang Qin [b], Hui Hu [c]

[a] School of Aeronautics and Astronautics, Shanghai Jiao Tong University, Shanghai 200240, China
[b] School of Energy Science and Engineering, Harbin Institute of Technology, Heilongjiang 150001, China
[c] Department of Aerospace Engineering, Iowa State University, Ames, IA 50010, United States

ARTICLE INFO

Keywords:
Film cooling
Vortex venerator (VG)
Counter-rotating vortex pair (CRVP)
Anti-counter-rotating vortex pair (anti-CRVP)
Pressure sensitive paint (PSP)
Particle image velocimetry (PIV)

ABSTRACT

In this study, the placement of a micro-vortex generator (VG) upstream of the film cooling hole is proposed to improve the film cooling performance. The film cooling effectiveness and flow characteristics at three blowing ratios (M = 0.2, 0.4, and 0.8) are measured by using pressure-sensitive paint (PSP) and particle image velocimetry (PIV), respectively. The results indicate that the VG upstream of the cooling hole can improve the film cooling performance, and the effect is more pronounced at high blowing ratios (M = 0.4 and 0.8). Flow field measurements reveal that an anti-counter-rotating vortex pair (anti-CRVP) is generated by the upstream VG, counteracting the detrimental effects of the counter-rotating vortex pair (CRVP) induced by the coolant jet. The detachment of the coolant jet from the test surface is significantly suppressed at high blowing ratios, and the coverage of the cooling gas in the spanwise direction is extended due to the anti-CRVP induced by the VG. In addition, the influences of the VG height and the distance between the VG and the cooling hole are investigated to obtain the optimal VG geometry to achieve high film cooling efficiency.

1. Introduction

Gas turbine engines are widely used in the energy and transportation industries. Higher performance of gas turbine engines is urgently needed due to economic and environmental requirements. Thermodynamic analysis has shown that the thermal efficiency of gas turbines can be improved by raising the turbine inlet temperature [1–2]. The inlet temperature of advanced gas turbines exceeds the melting point of the turbine blade material; thus, cooling methods, such as internal cooling, impinging cooling, film cooling, and combined cooling, have been utilized to protect the hot components of gas turbines from melting and corrosion. Film cooling has been one of the most important cooling strategies of gas turbines for decades. Therefore, improving the film cooling efficiency to reduce energy loss caused by coolant bleeds is crucial.

Film cooling is intrinsically an inclined jet-in-crossflow (JICF) problem. Numerous numerical simulations [3–4] and experimental investigations [5–8] have been conducted to explore the flow characteristics of the JICF. A review by Mahesh [9] showed that the complex flow structures of the JICF include jet shear-layer vortices around the perimeter of the jet, horseshoe vortices wrapping around the base of the jet, a counter-rotating vortex pair (CRVP) in the jet, and wake vortices downstream of the jet. The CRVP is thought to be the most crucial vortex structure affecting film cooling performance. It was found that the CRVP promotes the entrainment of the jet into the main flow, leading to a reduction in the film cooling performance.

A large number of studies have been conducted to seek new design to enhance the film cooling performance. A shaped hole with an expanded diffuser-type exit was first reported by Goldstein et al. [10], representing a major advancement of gas turbine engines. The development of shaped holes was summarized and reviewed by Bunker [11]. The diffuser-type exit can reduce the consumption of coolant gas and exhibits improved surface coverage in the spanwise direction. Haven et al. [12] found that an anti-counter-rotating vortex pair (anti-CRVP), rotating in the opposite direction of the CRVP, was generated in the flow field of the shaped hole. This anti-CRVP can weaken the strength of the CRVP induced by the coolant jet, leading to a better surface attachment of the jet flow. Due to the advantages of shaped holes, several hole geometries were proposed to further improve the film cooling performance, such as the converging slot-hole [13–14], cratered hole [15], and trenched hole [16].

Another strategy to improve the film cooling performance is based on the internal geometry design of the cooling hole. The vortex systems

* Corresponding author.
E-mail address: tianwei@sjtu.edu.cn (W. Tian).

https://doi.org/10.1016/j.expthermflusci.2021.110410
Received 19 January 2021; Received in revised form 21 March 2021; Accepted 26 March 2021
Available online 3 April 2021

Nomenclature

C_{o_2}	Mass concentration of oxygen molecules
D	Film cooling hole diameter
E_c	Eckert number of the main flow
I	Momentum flux ratio of coolant flow to mainstream
L	Distance between the trailing edge of the VG and the center of downstream film cooling hole
Le	Lewis number, $Le = \alpha/D_s$, where α is the thermal diffusivity and D_s is the mass diffusion coefficient
M	Blowing ratio,$\rho_C U_C/\rho_\infty U_\infty$
MW	Molecular weight ratio of the coolant gas to the mainstream gas
Re_D	Reynolds number based on the diameter of the film cooling hole
Tu	Turbulence intensity of the main flow
U	Mainstream velocity
h	Height of the vortex generator
l	Entry length of the cooling hole
l_{VG}	Length of the vortex generator
p_{o_2}	Partial pressure of oxygen
s	Spanwise pitch between the adjacent holes
w	Width of the vortex generator
β	Injection angle of the cooling hole
η	Film cooling effectiveness
δ	Boundary layer thickness
δ_1	Displacement thickness of the boundary layer
λ_{ci}	Swirling strength of the vortex

Subscript

ave, span	Spanwise averaged
∞	Inlet condition
c	Coolant flow condition
aw	Adiabatic wall

Acronyms

anti-CRVP	Anti-counter-rotating vortex pair
CRVP	Counter-rotating vortex pair
VG	Vortex generator

generated inside the hole before ejection are considered in this strategy. For example, Vogel [17] demonstrated that a left-curved inflow generated a vortex system inside the hole that counter-rotated against the external CRVP. This additional vortex system significantly reduces the strength of the CRVP and prevents the detachment of the jet flow from the surface. Furthermore, using two or more holes is also an effective method to improve film cooling performance. Kuster et al. [18] introduced a double-jet film cooling (DJFC) concept to establish an anti-CRVP through two neighboring cooling holes with compound angles. Subsequently, a Nekomimi cooling hole [19] was proposed to achieve the appropriate supply of cooling gas based on the DJFC concept. Heidmann and Ekkad [20] proposed an "anti-vortex" film cooling concept, in which two branched holes are drilled on both sides of the main hole. The vortices generated by the two branched holes effectively counteract the detrimental CRVP ejected from the main hole. In addition, a novel sister hole structure was numerically investigated by Ely and Jubran [21–22]. In this concept, the two sister holes were placed slightly downstream of the main cooling hole. The results indicated that the CRVP ejected from the main hole was impaired substantially by the two sister holes, leading to a significant improvement of film cooling performance.

In addition to the above cooling hole designs, strategies related to surface restructuring around the cooling hole were proposed in recent years to improve the film cooling performance. Lu et al. [23] proposed placing a row of film cooling holes into a surface trench to modify the interaction between the boundary layer and the jet flow. Na and Shih [24] placed a two-dimensional ramp with a backward-facing step in front of the coolant hole. The simulation results showed that the approaching boundary layer flow was deflected away from the surface, and the interaction of the boundary layer flow and coolant jet occurred far away from the surface. The laterally averaged film cooling effectiveness was improved at least two-fold by the ramp. More recently, a three-dimensional vortex generator (VG) that generates opposite vortex pairs to eliminate the negative effects of the CRVP was proposed by Rigby and Heidmann [25]. Subsequently, Zaman et al. [26–27] placed a VG downstream of the inclined jet flow and experimentally demonstrated the effectiveness of a downstream VG for preventing lift-off of a jet flow. Similar results were obtained by Shinn and Vanka [28] in a large eddy simulation (LES). Furthermore, Song et al. [29] experimentally investigated the effects of the inclination angle (20°, 30°, and 40°) and blowing ratio (M = 0.5, 1.0, and 1.5) on the film cooling performance when a VG was placed downstream of the cooling hole. It was found that the strong downwash effect of the vortex system generated by the VG significantly reduced the lift-off tendency of the jet flow, thereby improving the film cooling performance.

The above studies indicate that the VG geometry can enhance the film cooling effectiveness. However, most previous studies placed the VG downstream of the film cooling holes, thus the VG should be high enough to ensure that it can interact with the jet flow under high blowing ratios. In fact, the VG heights generally exceeded $0.75D$ (D is the diameter of the cooling hole) in the previous studies, which leads to a high pressure loss. If the VG was placed in front of the cooling hole and faced the high-speed incoming flow, the resulting vortex pairs should be stronger than that generated by VG placed in the low-speed wake region downstream of the jet flow. In addition, the approaching hot gas in the main flow might be deflected away from the surface if the VG was placed upstream of the cooling hole. Based on these assumptions, a VG with lower height ($h = 0.25D$ and $0.5D$) is placed upstream of the film cooling hole to investigate if the VG height can be decreased without losing the film cooling efficiency. The experimental study is conducted in a low-speed wind tunnel located at Shanghai Jiao Tong University. A pressure-sensitive paint (PSP) technique based on the analogy of heat and mass transfer [30–31] is utilized to measure the distribution of the adiabatic film cooling effectiveness on the test surface. The flow features are comprehensively measured using two-dimensional particle image velocimetry (2D-PIV) and stereoscope particle image velocimetry (SPIV). The measured flow field characteristics are correlated with the PSP measurements to elucidate the effects of the upstream VG structure on the film cooling performance.

2. Experimental setup

2.1. Experimental apparatus and test model

The experimental investigation was conducted in a low-speed wind tunnel located at the School of Aeronautics and Astronautics in Shanghai Jiao Tong University. The wind tunnel has an optically-transparent test section with a cross-section of 250 mm × 125 mm. The maximum flow velocity in the test section can reach 40 m/s. A honeycomb and screen structure installed upstream of the contraction section ensure a uniform low-turbulence incoming flow in the test section. The turbulence level of the incoming flow was within 0.5%. The mainstream velocity in all test cases was $U_\infty = 20m/s$. As indicated by Baldauf and Scheurlen [32], the Reynolds number based on the diameter of film cooling hole (Re_D) for

real gas turbine engine applications is approximately ranging from 10^4 to 10^5. Anderson et al. [33] indicated that the Re_D is within a range of $(0.5\ 4) \times 10^4$ for a gas turbine operating under real condition. In the present study, the Reynolds number based on the diameter of the film cooling hole was $Re_D = 1.6 \times 10^4$, which is in the range of the typical Reynolds number to investigate the film cooling of gas engine turbine blades. The boundary layer profiles measured just upstream of the cooling holes for the baseline case (i.e., without a VG placed on the test plate) is shown in Fig. 1. It is observed that the boundary layer profile is in good agreement with the 1/7th power law, indicating that the incoming flow is a fully-developed turbulent flow. The turbulent boundary layer thickness was estimated based on the velocity profile shown in Fig. 1; it was approximately 1.52D.

The test model of the film cooling holes with the upstream VGs is shown in Fig. 2. A row of 5 discrete circular holes with the same diameters of $D = 6.0mm$ was designed to inject coolant gas over a flat plate with an injection angle of $\beta = 30^{\circ}$. The entry length of the cooling holes was $l = 5D$. The spanwise pitch between the adjacent holes was set to be $s = 3D$, which is identical to the typical spacing between coolant holes in the spanwise direction for real gas turbine engine [2]. The VGs were placed upstream of each film cooling hole, and the axial centerline of the VGs coincided with those of the cooling holes. The length and width of the VG were fixed at $l_{VG} = 2D$ and $w = 1.5D$, respectively. As described in the introduction, two VG heights ($h = 0.25D$ and $0.5D$) were tested in the experiments. In addition, the distance between the trailing edge of the VG and the center of the cooling hole was defined as L. Two distances ($L = D$ and $2D$) were investigated to evaluate the effects of the VG location on the film cooling effectiveness. As shown in Fig. 2, for the distance of $L = D$, the trailing edge of the VG contacts the leading edge of the cooling hole. Three blowing ratios ($M = \rho_C U_C / \rho_\infty U_\infty = 0.2, 0.4, 0.8$, where ρ_C and U_C are the density and velocity of the coolant flow, and ρ_∞ is the density of the main flow) were adopted to investigate the effects of the blowing ratio on the performances of the upstream VGs.

2.2. PSP technique to measure the film cooling effectiveness

Adiabatic film cooling effectiveness η is generally defined as:

$$\eta = \frac{T_\infty - T_{aw}}{T_\infty - T_c} \tag{1}$$

where T_∞ is the temperature of the main flow, T_{aw} is the adiabatic wall

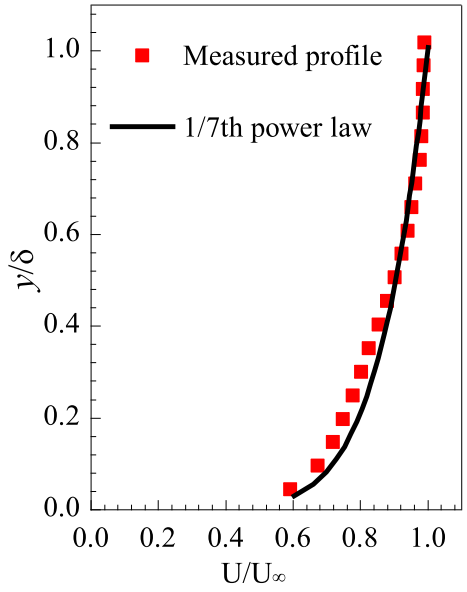

Fig. 1. Measured boundary layer profile of the mainstream over the test plate.

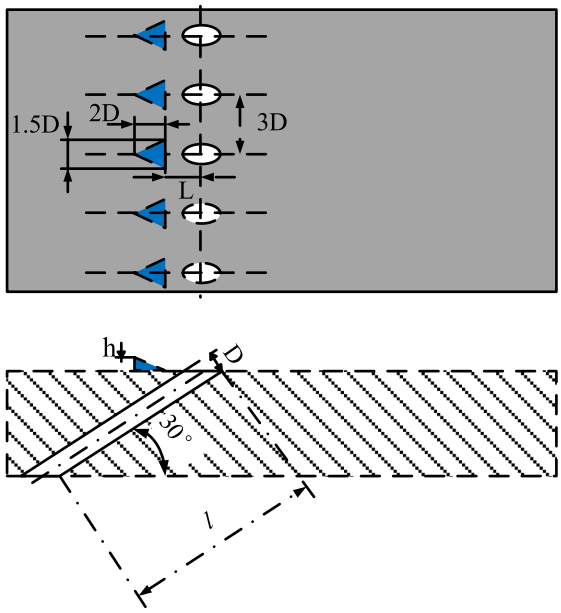

Fig. 2. The schematic of the film cooling configuration with the VG.

temperature of the test surface, and T_c is the temperature of the coolant stream. The primary challenge in obtaining adiabatic film cooling effectiveness is the measurement of adiabatic wall temperature because the heat conduction in a test model cannot be entirely avoided during the experiments.

In the present study, instead of measuring adiabatic wall temperature, a PSP technique operating under isothermal condition was used to measure the film cooling effectiveness based on the analogy of heat and mass transfer [34–35]. Johnson et al. [36] indicated that the PSP based cooling effectiveness measurements can avoid the problems related to the effects of heat conduction in the test model on the measurement of the adiabatic wall temperature. In addition, as described by Shadid and Eckert [34], the differential equations regarding heat and mass transfer can be treated as analogous if the Lewis number ($Le = \alpha / D_s$, where α is the thermal diffusivity and D_s is the mass diffusion coefficient) was approximately 1.0, which is the case of the present study.

For the PSP measurements, the plate surface is coated with a layer of oxygen-sensitive paint, consisting of luminophore molecules and a gas-permeable polymeric binder. When excited by ultraviolet (UV) light, the luminophore molecules emit photoluminescence with a longer wavelength when returning to the ground state from the excited state. However, the emission of luminophore molecules can be inhibited due to the existence of surrounding oxygen molecules. This phenomenon is called oxygen quenching, where the intensity of the photoluminescence is inversely proportional to the concentration of the local oxygen. Consequently, the concentration of oxygen molecules can be calculated based on the recorded light intensity and a calibration procedure.

For the PSP based cooling effectiveness measurements, air flow is typically used to simulate the mainstream, while oxygen-free gas (e.g., nitrogen or carbon dioxide) is supplied as the coolant stream. The oxygen-free gas ejected through the coolant holes prevents the oxygen molecules in mainstream (i.e., air flow) from reaching the surface of interest. The film cooling effectiveness is determined in terms of the oxygen concentration over the protected surface. Thus, by replacing the temperature in Eq. (1) with the oxygen concentration, the film cooling effectiveness can be expressed as:

$$\eta = \frac{C_{O_2,main} - C_{O_2,mix}}{C_{O_2,main} - C_{O_2,coolant}} = \frac{C_{O_2,main} - C_{O_2,mix}}{C_{O_2,main}} \tag{2}$$

As indicated by Charbonnier et al. [37], by choosing an oxygen-free coolant gas whose molecular mass differs distinctly from that of the

mainstream, the film cooling effectiveness based on the measurement of the partial pressure of oxygen should be calculated as:

$$\eta = 1 - \frac{1}{\left[\left(p_{o_2}\right)_{air}/\left(p_{o_2}\right)_{mix} - 1\right]MW + 1} \quad (3)$$

where MW is the molecular weight ratio of the coolant gas to the mainstream gas. $(p_{o_2})_{air}$ and $(p_{o_2})_{mix}$ are the partial pressures of oxygen measured in the air and on the film cooling surface, respectively.

The pressure terms in Eq. (3) can be determined by using the recorded intensity of the emitted light, which is a function of the partial pressure of oxygen (i.e., local oxygen concentration). The function describing the relationship between the normalized intensity and partial pressure can be determined by a PSP calibration procedure. More information on the details of the PSP technique, such as image processing, and calibration process can be found in [38].

Fig. 3 shows the experimental setup for the PSP measurements. A constant UV light with a wavelength of 405 nm was used as the excitation light source for the PSP measurements. A 14-bit charge-coupled device (CCD) camera (PCO2000, Cooke Corp.) with a 610 nmlong-pass filter was used to record the photoluminescence light emitted by the luminophore molecules in the PSP paint. The PSP used in this study was Unicoat (ISSI), which has a low sensitivity to temperature change (1.3%/°C). The coolant flow temperature was kept equal to that of the main flow to reduce the influence of temperature, and the temperature fluctuation during the measurements was less than 0.5°C.

In the present study, an interrogation window of 9 × 9 pixels with 50% overlap was used in image processing to minimize the effects of random noise in the images. The acquired images had a magnification of 0.07 mm/pixel, resulting in a spatial resolution of 0.32 mm for the PSP measurements. As indicated by Johnson and Hu [36], the PSP based cooling effectiveness measurement has a varying degree of uncertainty, which directly depends on the local behavior of the mixing process between the mainstream and coolant flows. The measured film cooling effectiveness with error bar along the centerline of coolant hole for the baseline case (without upstream VG) is plotted in Fig. 4. The absolute uncertainty was found to increase continuously with the decrease of film cooling effectiveness, which is approximately 0.018 for η = 0.7 in the region near the coolant hole and is 0.028 for η = 0.3 in the far field region away from the coolant hole. The corresponding relative uncertainty varies from 3% to 9% with the increase of distance downstream the coolant hole.

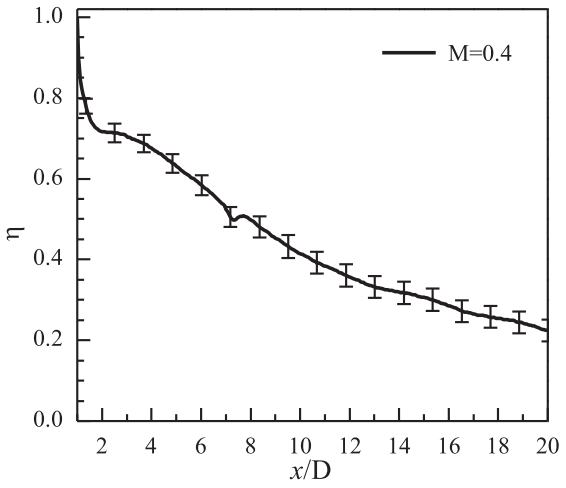

Fig. 4. Uncertainty of measured film cooling effectiveness along the centerline of the coolant hole (baseline case, M = 0.4).

2.3. Flow field measurements using 2D-PIV and SPIV

In this study, the flow field measurements were conducted using 2D-PIV and SPIV to quantify the mixing process of the coolant and the mainstream flow downstream of the film cooling holes. During the PIV measurements, the incoming airflow and the coolant flow (i.e., N_2 in this study) were both seeded with oil droplets (diameter of approximately 1μm) generated by seeding generators. The measured plane was illuminated by a double-pulsed Nd:YAG laser (Vlite-380, Beamtech) with a pulse energy of 380mJ at 10 Hz repetition rate. The thickness of the laser sheet shaped by a set of spherical and cylindrical lenses was approximately 1.0 mm in the measurement region. The image acquisition devices used in the PIV measurements were 14-bit CCD cameras (PCO2000, Cooke Corp.) with a resolution of 2048 × 2048 pixels. The cameras and double-pulsed Nd:YAG laser were connected to a digital delay generator (Berkeley Nucleonics 575), which controlled the timing

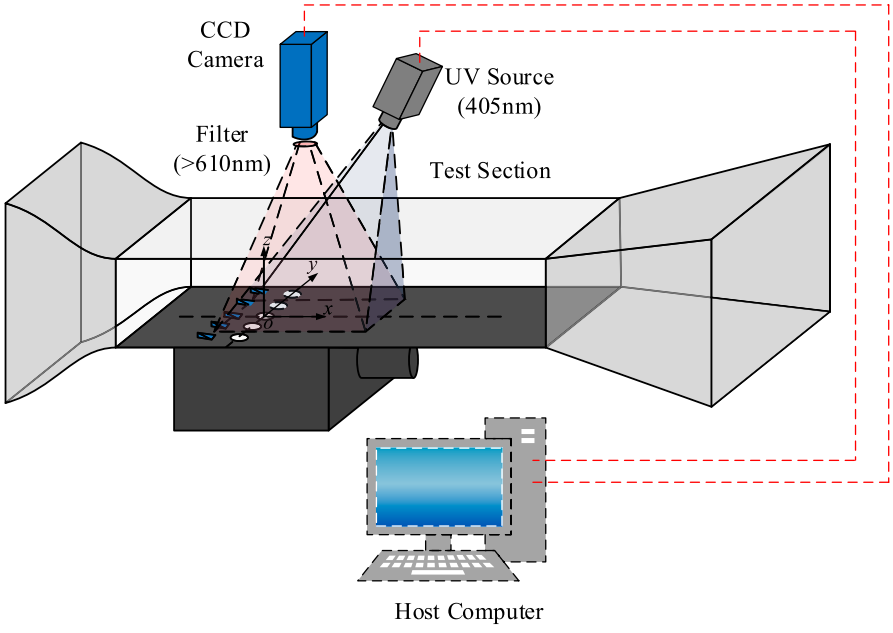

Fig. 3. Experimental setup for the PSP measurements.

of the laser illumination and image acquisitions.

The diagram of the measurement setup is shown in Fig. 5. PIV measurements were conducted to measure velocity components from two orthogonal views: vertical streamwise ($x-z$) plane and vertical spanwise ($y-z$) plane. As shown in Fig. 5, while 2D-PIV was performed in $x-z$ plane passing through the centerline of the middle film cooling hole on the test plate (i.e.,$y = 0$), SPIV was conducted in two $y-z$ planes (i.e., x/D = 3 and 6 downstream the center of film cooling hole).

A grid target placed in the laser sheet is used to calibrate the 2D-PIV measurement, which provides a scale factor by converting the length scale from the measurement plane to the image plane. S-PIV calibration was performed by following a general in-situ multi-plane procedure described by Raffel et al. [39]. After PIV image acquisition, the instantaneous PIV velocity vectors were obtained by a frame-to-frame cross-correlation technique with an interrogation window of 24 × 24 pixels. An effective overlap of 50% of the interrogation windows was utilized in the PIV image processing. Consequently, the spatial resolution for 2D-PIV and SPIV measurements were 0.26 mm and 0.31 mm, respectively. After the instantaneous velocity vectors were determined, the ensemble-averaged flow quantities, such as the mean velocity ($\overline{u}$, $\overline{v}$, $\overline{w}$) and the spanwise vorticity (ω_y) for the 2D-PIV measurements and the streamwise vorticity (ω_x) for the SPIV measurements were obtained from a sequence of 900 frames of the instantaneous PIV measurements. The uncertainty level for the PIV measurements was within 3% for the instantaneous velocity vectors and that of the ensemble-averaged flow quantities, such as the vorticity distributions, was approximately 10%.

3. Results and discussion

3.1. Effects of the VG on the film cooling effectiveness

The distribution of film cooling effectiveness on the test plate with the VG mounted upstream of the cooling hole is shown in Fig. 6. The baseline cases without the upstream VG are also plotted for comparison. For the baseline cases, the film cooling effectiveness increases with an increase in the blowing ratio from 0.2 to 0.4. However, it should be noted that in the region near the hole exit, the film cooling effectiveness at M = 0.4 is lower than that at M = 0.2, indicating that the coolant jet has slightly separated from the surface. With a further increase in the blowing ratio, the decrease in the film cooling effectiveness caused by the separation of the coolant streams exceeds the benefits of increasing the cooling gas flux. It can be seen in Fig. 6(e) that the film cooling performance deteriorates rapidly as the blowing ratio increases to M = 0.8.

After installing the VG in front of the cooling hole, the coverage area of the coolant gas is larger than that in the baseline case, resulting in a better film cooling performance at all three blowing ratios, as shown in Fig. 6. For M = 0.2, a higher surface coverage of the coolant gas is observed in the spanwise direction in Fig. 6(b). The cooling film becomes thinner as the coolant gas expands in the spanwise direction. If the cooling film is too thin, its ability to resist the influx of the main flow on the surface is weakened. Since the cooling film is very thin at a low blowing ratio (e.g., M = 0.2), a further reduction in the film thickness caused by the presence of the VG deteriorates the film cooling performance as the coolant flow moving downstream. Therefore, as shown in Fig. 6(a) and (b), the film cooling effectiveness decreases slightly faster than that of the baseline case in the streamwise direction.

At a blowing ratio of M = 0.4, the cooling film is relatively thick; therefore, the expansion of the coolant gas in the spanwise direction has no adverse effect on the film cooling performance in the streamwise direction. In addition, the film cooling effectiveness near the hole exit is higher than that of the baseline case, indicating that the coolant jet is still attached to the surface at this blowing ratio. Thus, the cooling gas is utilized more efficiently due to the presence of the VG. It can be observed in Fig. 6(c) and (d) that the coverage of the coolant gas is highly improved by the upstream VG in both the spanwise and streamwise directions.

The most significant improvements in the film cooling effectiveness caused by the upstream VG occur at a high blowing ratio (e.g., M = 0.8). The separation of the coolant jet from the plate surface is significantly inhibited by the upstream VG. The region with relatively high film cooling effectiveness is much larger in the spanwise and streamwise directions compared with the narrow and short coverage area of the coolant gas in the baseline case. The results in Fig. 6 suggest that the VG installed upstream of the cooling hole significantly improves the film cooling effectiveness, and this effect is more pronounced at relatively high blowing ratios (e.g., M = 0.4, 0.8). In addition, the coverage range of coolant gas in spanwise direction was found to be dominated by the upstream VG structure. Therefore, the VG geometry can be used to control the expansion of the coolant gas within a wide range of the blowing ratio.

The comparisons of the centerline and spanwise-averaged film cooling effectiveness between the VG and the baseline cases are plotted in Fig. 7 to quantify the effects of the upstream VG on the film cooling performance. At a relatively low blowing ratio (e.g., M = 0.2), with the continuous mixing of the coolant gas with the main flow downstream of the coolant hole, the magnitudes of both the centerline and spanwise-averaged film cooling effectiveness decrease gradually with an increasing downstream distance. The VG presence results in a decrease in the centerline film cooling effectiveness of 7–20% compared with the baseline case. However, the spanwise-averaged film cooling effectiveness is improved by 11–43% due to the presence of upstream VG. This finding indicates that the spreading of the coolant gas in the spanwise direction is wider and more uniform in the VG case, which agrees with the distributions shown in Fig. 6(a).

At a blowing ratio of M = 0.4, both the centerline and spanwise-

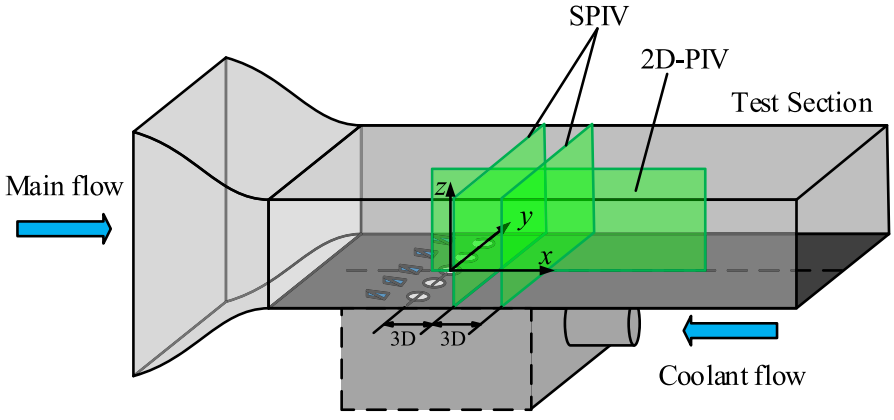

Fig. 5. Experimental setup for the 2D-PIV and SPIV measurements.

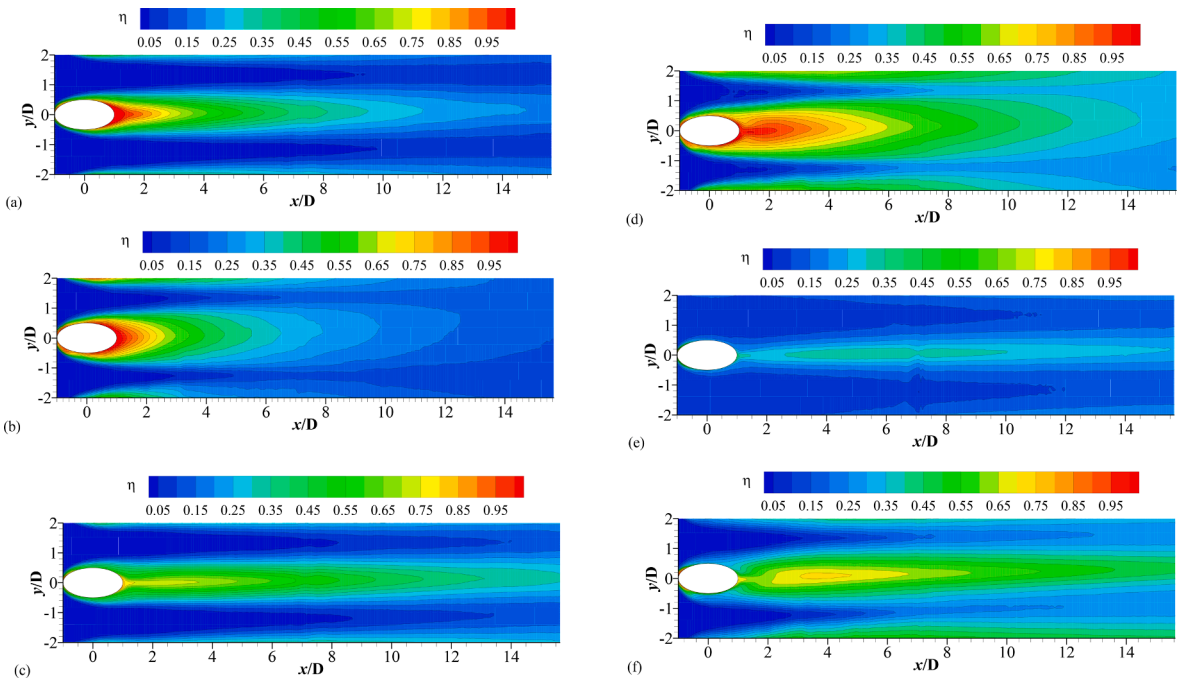

Fig. 6. Comparison of the film cooling effectiveness between the baseline and the VG cases (a) M = 0.2, baseline; (b) M = 0.2, VG; (c) M = 0.4, baseline; (d) M = 0.4, VG; (e) M = 0.8, baseline; (f) M = 0.8, VG.

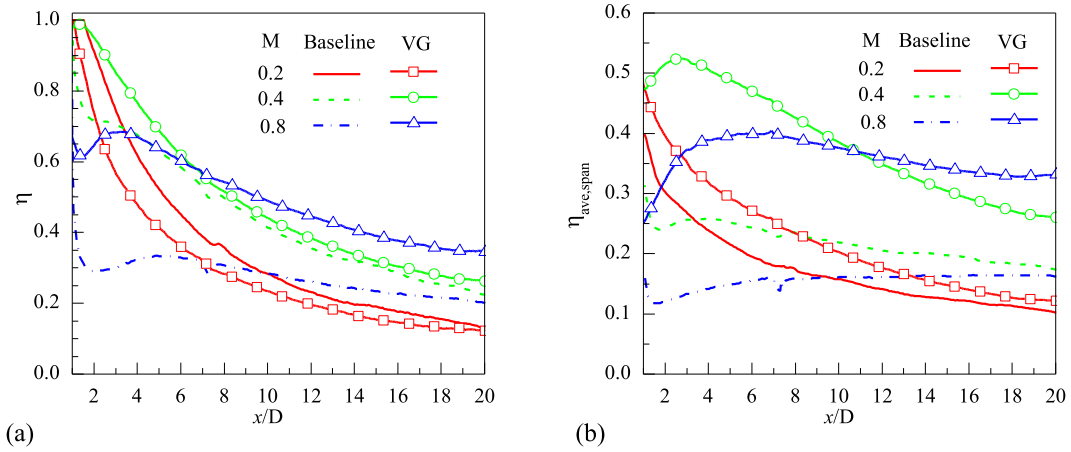

Fig. 7. Comparison of the (a) centerline and (b) spanwise-averaged film cooling effectiveness between the VG and the baseline cases.

averaged film cooling effectiveness values are higher than those of the baseline case. The difference in the centerline film cooling effectiveness between the cases is especially large in the region of $x/D < 6$ because the separation of the coolant flow in the baseline case is eliminated after the VG installation. In addition, the VG has a more substantial effect on the spanwise-averaged film cooling effectiveness than the centerline film cooling effectiveness, i.e., a 40–113% increase in effectiveness compared with the baseline case.

At the blowing ratio of M = 0.8, the centerline film cooling effectiveness of the baseline case decreases rapidly near the hole exit (i.e., $x/D < 2$) and then gradually increases in the region of $2 < x/D < 5$. With a further increase in the downstream distance, the film cooling effectiveness decreases gradually due to the continuous mixing of the coolant gas with the main flow. Both the centerline and spanwise-averaged film cooling effectiveness values increase significantly after installing the VG in front of the film cooling hole. As shown in Fig. 7(a), the decline in the centerline film cooling effectiveness near the hole exit is not as large as that of the baseline case. In addition, the distance of the initial decrease followed by an increase in the centerline film cooling effectiveness (i.e., $x/D < 3.0$) is much shorter than that of the baseline case. These results indicate that the separation of the coolant flow from the surface has been substantially suppressed by the upstream VG.

3.2. *Effects of the VG on the flow structure downstream of the film cooling hole*

3.2.1. *Flow characteristics in the streamwise plane measured by 2D-PIV*

High-resolution PIV measurements were conducted to determine the detailed flow field, investigate the mixing process between the coolant jet and the main flow, and explore the underlying mechanism responsible for the improvements in the film cooling performance by placing the VG upstream of the cooling hole. The flow field measurements in the streamwise plane (i.e., $z = 0$) for the baseline and the VG cases at blowing ratios of M = 0.2, 0.4, and 0.8 are shown in Figs. 8–10. At a relatively low blowing ratio of M = 0.2, the cooling streams injecting through the inclined hole remain attached to the test surface in both the

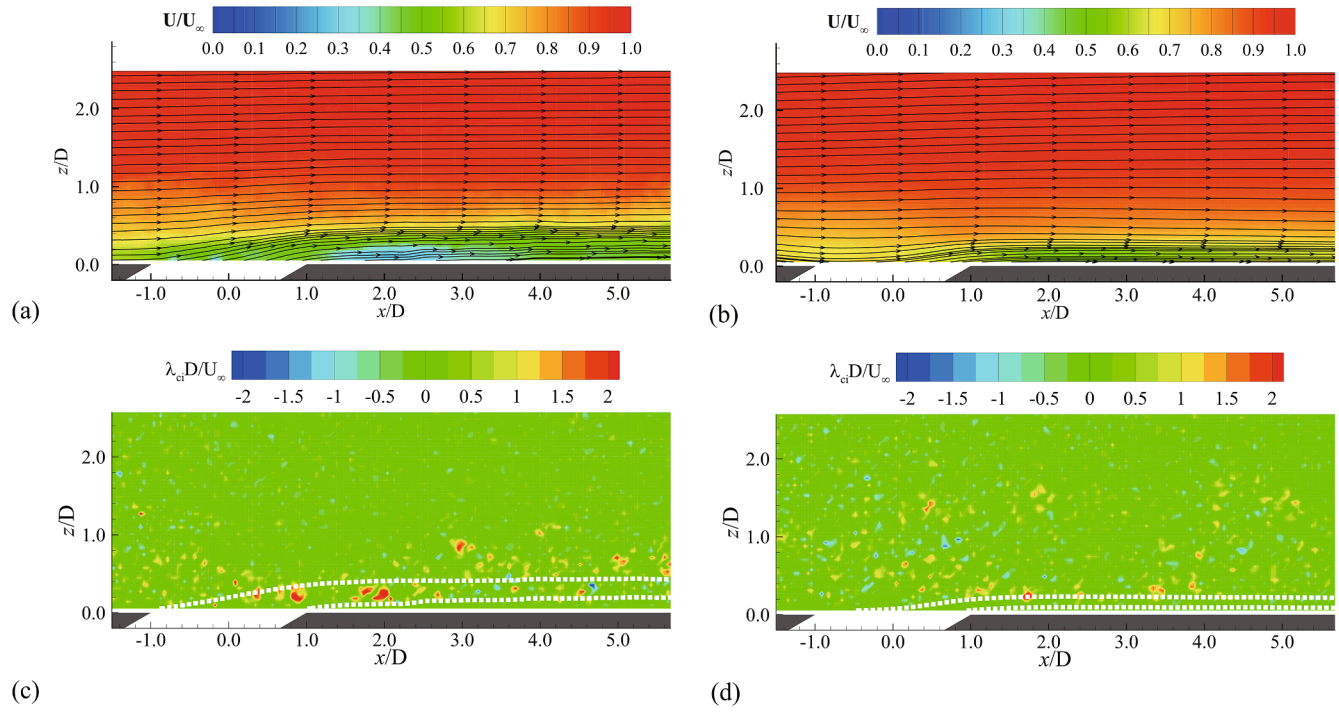

Fig. 8. Flow field measured in the streamwise plane for the baseline and the VG cases at the blowing ratio of M = 0.2. (a) Ensemble-averaged velocity, baseline case; (b) Ensemble-averaged velocity, VG case; (c) Instantaneous swirling strength, baseline case; (d) Instantaneous swirling strength, VG case.

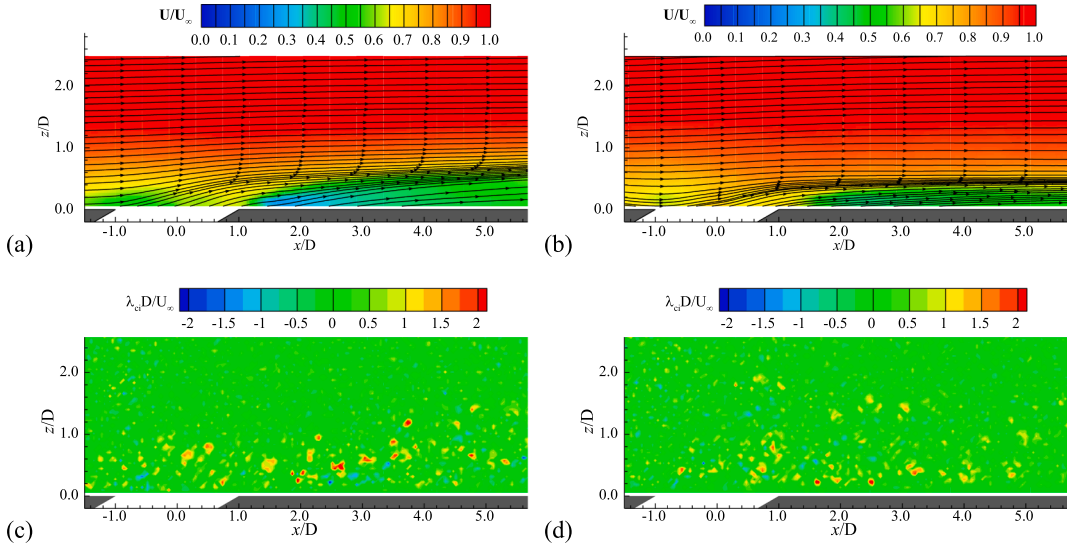

Fig. 9. Flow field measured in the streamwise plane for the baseline and the VG cases at the blowing ratio of M = 0.4. (a) Ensemble-averaged velocity, baseline case; (b) Ensemble-averaged velocity, VG case; (c) Instantaneous swirling strength, baseline case; (d) Instantaneous swirling strength, VG case.

baseline and the VG cases. As shown in Fig. 8(b), the thickness of the cooling film is reduced by the presence of the upstream VG structure. The thin layer of coolant gas cannot prevent the influx of the main flow on the surface. As a result, the centerline film cooling effectiveness is not improved by the VG at the blowing ratio of M = 0.2, as shown in Fig. 7 (a).

At the blowing ratio of M = 0.4, the detachment of the coolant jet from the surface can be observed near the hole exit for the baseline case, resulting in a lower centerline film cooling effectiveness than for M = 0.2. After installing the VG upstream of the cooling hole, the downwash flow induced by the VG prevents the coolant gas from lifting off the surface. It can be seen in Fig. 9(b) that the separation of the coolant jet from the surface has disappeared, leading to an increase in the centerline film cooling effectiveness in the region of $x/D < 3.8$.

With a further increase in the blowing ratio, the coolant gas rapidly moves away from the surface after being ejected from the cooling hole. The streamlines in Fig. 10(a) reveal that most of the coolant gas has penetrated into the mainstream flow, resulting in a very low film cooling performance on the test surface. As shown in Fig. 10(b), although the separation of the coolant gas is observed in the VG case, the downward deflection of the coolant flow streamlines is more apparent than in the baseline case due to the downwash flow induced by the upstream VG. The cooling stream is closer to the surface than in the baseline case. This change in the coolant flow highly improves the film cooling efficiency over the surface, as shown in Fig. 6(f) and 7.

In the film cooling flow fields, the shearing motions in the boundary

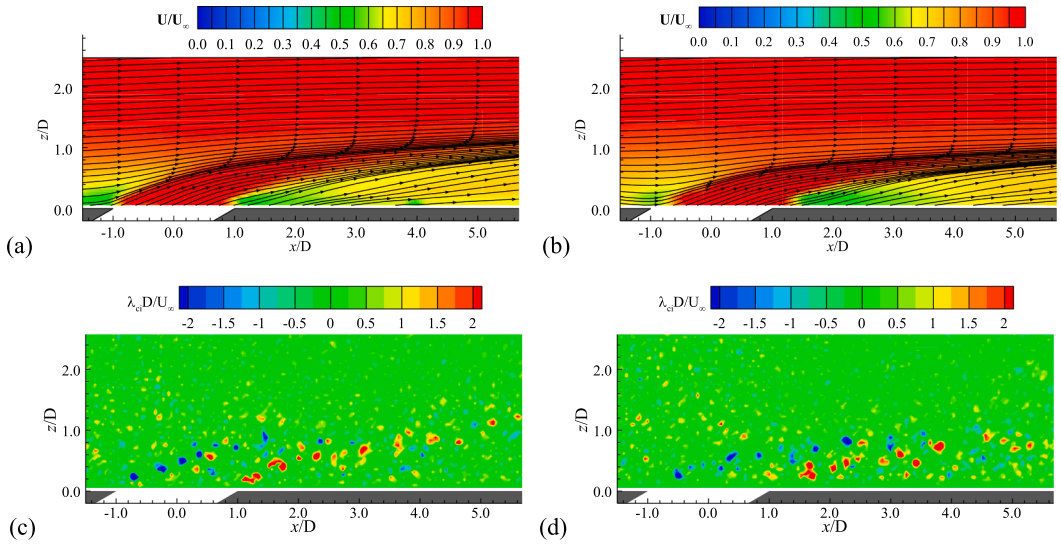

Fig. 10. Flow field measured in the streamwise plane for the baseline and the VG cases at the blowing ratio of M = 0.8. (a) Ensemble-averaged velocity, baseline case; (b) Ensemble-averaged velocity, VG case; (c) Instantaneous swirling strength, baseline case; (d) Instantaneous swirling strength, VG case.

layer flow are the dominant contributors to vorticity. In the vorticity plots, it nearly impossible to distinguish the swirling motions of the vortex structures from the strong shearing motions. In this study, we use the swirling strength to visualize the vortex structures in the film cooling flow fields. Chong et al. [40] described the swirling strength as the imaginary part of the complex eigenvalue of the velocity gradient tensor; it can be used to distinguish between swirling motions and shear motions. As shown in Figs. 8 to 10, the instantaneous swirling strength reveals the mixing process of the coolant gas with the main flow. Unsteady vortex structures caused by Kelvin-Helmholtz instabilities are formed surrounding the coolant jet and shed periodically in the shear layer between the coolant flow and the main flow.

At a relatively low blowing ratio of M = 0.2, the shear layer between the cooling stream and the mainstream is only formed at the windward side because the coolant flow is attached to the test plate, resulting in the formation of Kelvin-Helmholtz vortices in this shear layer region. The streamlines originated from the leading and trailing edge of the film cooling hole were also plotted in Fig. 8(c) and (d). It can be seen that after mounting the VG upstream of the cooling hole, the coolant jet moves closer to the surface and the shear layer thickness is highly reduced. In addition, both the strength and the quantity of Kelvin-Helmholtz vortices in the shear layer are reduced compared to the baseline case.

At the blowing ratio of M = 0.4, the Kelvin-Helmholtz vortices on the lee side begin to appear in the baseline case due to the detachment of the cooling stream from the tested surface; this phenomenon is observed in the region near $x/D = 3$, as shown in Fig. 9(c). After installing the VG, the flow separation is suppressed, and the coolant gas remains attached to the surface. Therefore, the Kelvin-Helmholtz vortices are not observed on the lee side of the cooling stream in the VG case, as shown in Fig. 9(d).

At the blowing ratio of M = 0.8, the Kelvin-Helmholtz vortices on the lee side are observed in the baseline and VG cases due to the separation of the cooling stream from the tested surface. As the coolant flow moves downstream, the strength of the Kelvin-Helmholtz vortices decreases gradually due to the continuous mixing of the coolant gas with the main flow. The vortices on the windward side are maintained for a longer distance in the VG case than the baseline case, indicating that the upstream VG delays the mixing process of the coolant gas with the main flow, thereby increasing the film cooling efficiency. In addition, since the velocity of the coolant flow is higher than the surrounding mainstream velocity, the rotation direction of the Kelvin-Helmholtz vortices is opposite to that at the low blowing ratio. It is observed that the rotation direction of the Kelvin-Helmholtz vortices on the windward side changes from clockwise to counter-clockwise as the blowing ratio increases from M = 0.4 to M = 0.8.

3.2.2. *Flow characteristics in the cross-plane measured by SPIV*

As shown in Figs. 9 and 10, the coolant jet lifts off the surface and penetrates the mainstream at high blowing ratios, leading to a decrease in the film cooling effectiveness. As mentioned in the introduction, the CRVP in the streamwise direction is believed to be responsible for the poor film cooling performance at high blowing ratios. Thus, the streamwise vortices are vital for film cooling performance. In this study, a SPIV system was used to measure the flow fields in the cross-plane (i.e., the *y*-*z* plane) to reveal the generation and evolution of the streamwise vortex structures in the baseline and VG cases.

Fig. 11 shows the measurement results of the SPIV at $x/D = 3$ for the baseline and the VG cases at different blowing ratios. At a low blowing ratio (i.e., M = 0.2), the CRVP generated by the coolant jet is close to the surface and has a very low intensity. This behavior of the CRVP agrees with the streamline characteristics plotted in Fig. 8(a), indicating that the coolant jet remains attached to the surface after blowing out of the cooling hole. At relatively high blowing ratios (i.e., M = 0.4, 0.8), the CRVP is observed clearly in the plot of the swirling strength distribution in Fig. 11(c) and 11(e). It can be seen that the strength of the CRVP in the coolant jet is greatly enhanced with the increase of blowing ratio. Meanwhile, the CRVP was found to rapidly rise away from the surface at high blowing ratios due to the separation of coolant jet after being ejected from the cooling hole.

After installing the VG upstream of the cooling hole, apart from the CRVP generated in the coolant injection, an additional CRVP induced by the upstream VG is also observed. The rotation direction of the additional CRVP is opposite to that of the CRVP induced by the coolant injection; therefore, this additional vortex pair is referred to as the anti-CRVP. This vortex structure downstream of the triangular ramp-shaped structure was also reported by Zaman et al. [26–27] and Shinn and Vanka [28].

Due to the rotation direction of the anti-CRVP, a downwash flow occurs between the two vortices of the anti-CRVP, pushing the coolant jet closer to the surface and improving the film cooling performance. Besides, the existence of the anti-CRVP causes the coolant flow near the surface to move outward, promoting the spread of the coolant gas in the spanwise direction and resulting in better lateral coverage of the cooling

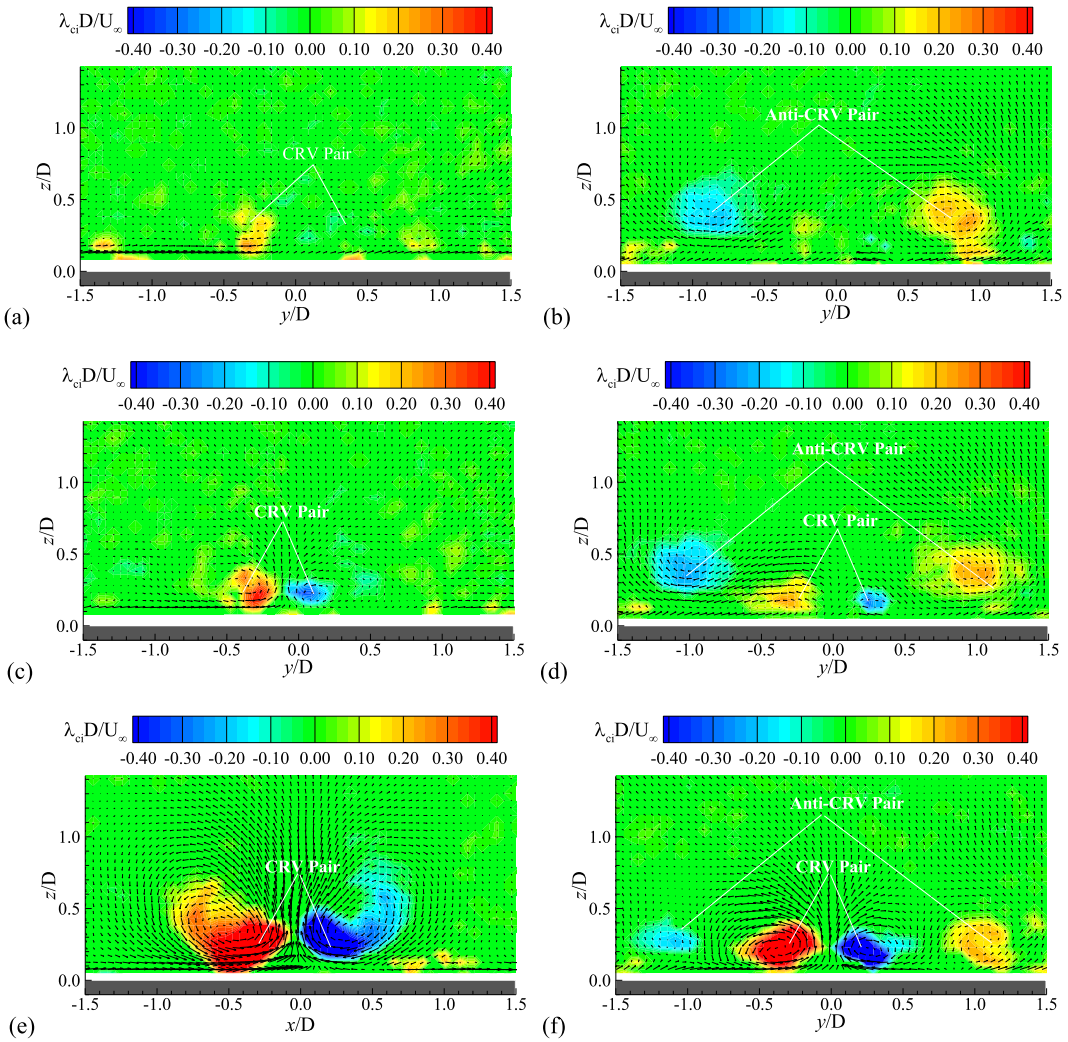

Fig. 11. Flow field in the cross-plane at $x/D = 3$ for the baseline cases and the VG cases at different blowing ratios. (a) M = 0.2, baseline case; (b) M = 0.2, VG case; (c) M = 0.4, baseline case; (d) M = 0.4, VG case; (e) M = 0.8, baseline case; (f) M = 0.8, VG case.

film compared with that of the baseline case. Therefore, it can be seen in Figs. 6 and 7(b) that the spanwise-averaged film cooling effectiveness is improved by the existence of the VG.

At a low blowing ratio (i.e., M = 0.2), the anti-CRVP dominates the flow structures in the cross-plane for the VG case since the CRVP induced by the coolant injection is weak. In contrast, faster spanwise spreading of the coolant gas is induced by the anti-CRVP, and the thickness of the cooling film near the centerline of the hole is decreased, resulting in a lower centerline film cooling effectiveness compared with that of the baseline case. At relatively high blowing ratios (i.e., M = 0.4, 0.8), the lifted CRVP is pushed back to the surface by the anti-CRVP, and the strength of the CRVP has decreased due to vorticity cancellation effect. In addition, the strength of the anti-CRVP decreases gradually with an increase in the blowing ratio as a result of a continuous enhancement of the vorticity cancellation effect between the CRVP and the anti-CRVP. Besides the vortex strength, the position of the vortices in the anti-CRVP also differs for different blowing ratios. As the blowing ratio increases, the anti-CRVP gradually moves closer to the surface, and the spacing between the two vortices in the anti-CRVP increases due to an increase in the strength of the CRVP generated by the coolant injection.

The streamwise vortex structures measured at two typical streamwise locations (i.e., $x/D = 3$ and 6) for the baseline and VG cases at a blowing ratio of M = 0.8 are shown in Fig. 12. It is observed that the flow structures downstream of the cooling hole are dominated by a large-scale streamwise vortex pair (i.e., CRVP) in the baseline case. As the downstream distance increases, the strength of the CRVP decreases due to turbulent mixing between the coolant gas and the main flow. After installing the VG in front of the hole, the anti-CRVP induced by the VG pushes the lifted CRVP back to the surface and weakens the strength of the CRVP. These interactions of the anti-CRVP and the CRVP suspend the detachment of the coolant jet from the surface, significantly enhancing the film cooling effectiveness.

3.3. *Effect of the VG height on the film cooling performance*

As described above, the film cooling effectiveness can be improved by the VG due to the generation of the anti-CRVP. It is expected that the increase of VG height enhances the strength of the anti-CRVP. However, the incursion of the VG into the main flow also becomes stronger, resulting in additional pressure loss. Thus, it is necessary to examine the effects of the VG height on the film cooling performance. It should be noted that the measurement results in Sections 3.1 and 3.2 were obtained using the VG with a height of $h = 0.5D$. This height is lower than that in previous studies where the VG was placed downstream of the cooling hole. Since the main purpose of this study is to investigate the possibility of decreasing the VG height, the film cooling effectiveness and flow field characteristics for the case with a VG height of $h = 0.25D$ was measured in this study. Fig. 13 shows the distribution of the film cooling effectiveness for the case with a VG height of $h = 0.25D$. As shown in Figs. 6 and 13, the film cooling performance decreases with a

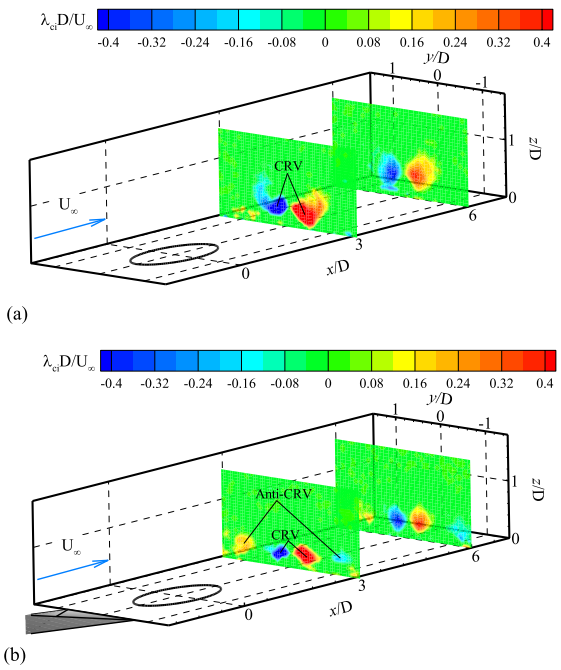

Fig. 12. Evolution of the streamwise vortex structures for (a) the baseline case and (b) the VG case at the blowing ratio of M = 0.8.

decrease in the VG height because the flow downwash and the anti-CRVP are weaker at a lower VG height. However, compared with the baseline case, the film cooling performance is also significantly improved by the VG with a lower height of h = 0.25D at different blowing ratios.

Fig. 14 shows the centerline and spanwise-averaged film cooling effectiveness extracted from Figs. 6 and 13. At a relatively low blowing ratio (i.e., M = 0.2), the centerline film cooling effectiveness is slightly lower, and the spanwise-averaged film cooling effectiveness is substantially higher than the baseline case for the VG height of h = 0.25D. The spanwise-averaged film cooling effectiveness is even higher than that of the case with VG height of h = 0.5D in the far downstream region (i.e., x/D > 11). At a high blowing ratio (i.e., M = 0.8), both the centerline and spanwise-averaged film cooling effectiveness decrease with a reduction in the VG height. In addition, the spanwise-averaged film cooling effectiveness is more sensitive than the centerline cooling effectiveness to the VG height, as shown in Fig. 14.

Fig. 15 shows the streamwise velocity distribution between the trailing edge of the VG and the center of the cooling hole at a blowing ratio of M = 0.8. The flow downwash can be observed near the leading edge of the cooling hole for the VG height of h/D = 0.5. However, this flow downwash phenomenon is less pronounced for the VG height of h/D = 0.25, as shown in Fig. 15(a). Therefore, the detachment of the coolant flow from the surface is not substantially hindered by the downwash flow, leading to a relatively lower centerline film cooling effectiveness at a lower VG height.

3.4. Effects of the streamwise distance between the VG and cooling hole on the film cooling performance

In addition to the VG height, the distance between the VG and the cooling hole is also investigated in this study. The previous results were obtained for VG locations of $L = 2D$. An additional VG location with a shorter distance upstream of the cooling hole (i.e., $L = D$) is selected to evaluate the effects of the VG location on the film cooling effectiveness. Fig. 16 compares the centerline and spanwise-averaged film cooling effectiveness between the two different VG streamwise locations. At a low blowing ratio (M = 0.2), the centerline film cooling effectiveness with a VG location of $L = 2D$ is close to that of the baseline case. In contrast, the spanwise-averaged film cooling effectiveness shows an improvement over the baseline case, and the values are even higher than those of the case with a VG location of $L = D$ in the downstream region of x/D > 7. As the blowing ratio increases to M = 0.8, it is observed in Fig. 16(c) and (d) that both the centerline and spanwise-averaged film cooling effectiveness values decrease with an increase in the upstream distance L. However, the VG location has a smaller influence on the film cooling effectiveness than the VG height. As shown in Fig. 16(a) and (b), a longer upstream distance of VG is beneficial at a low blowing ratio.

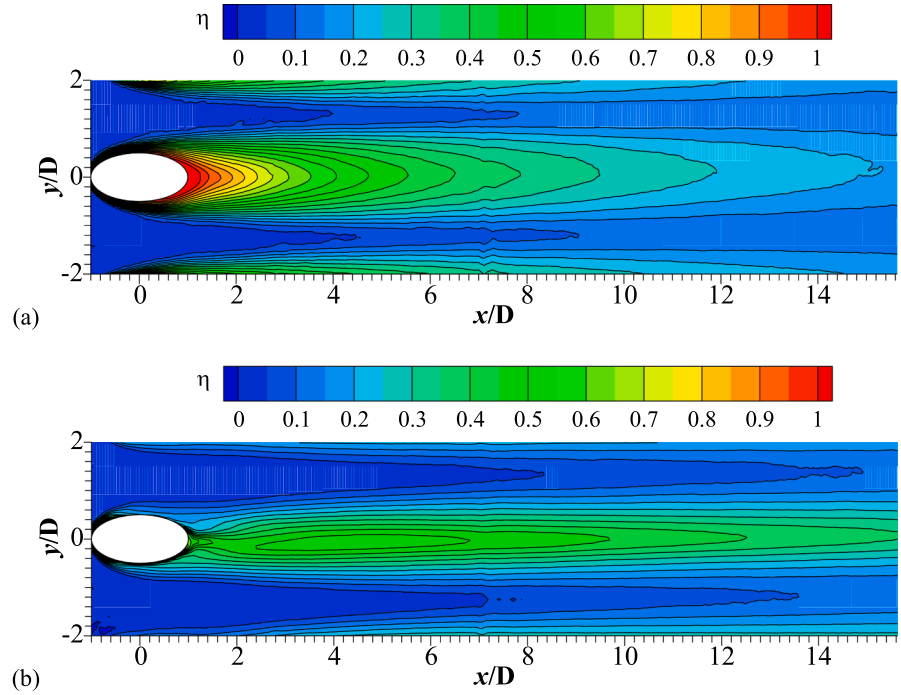

Fig. 13. Film cooling effectiveness for the cases with a VG height of h = 0.25D at blowing ratios of (a) M = 0.2 and (b) M = 0.8.

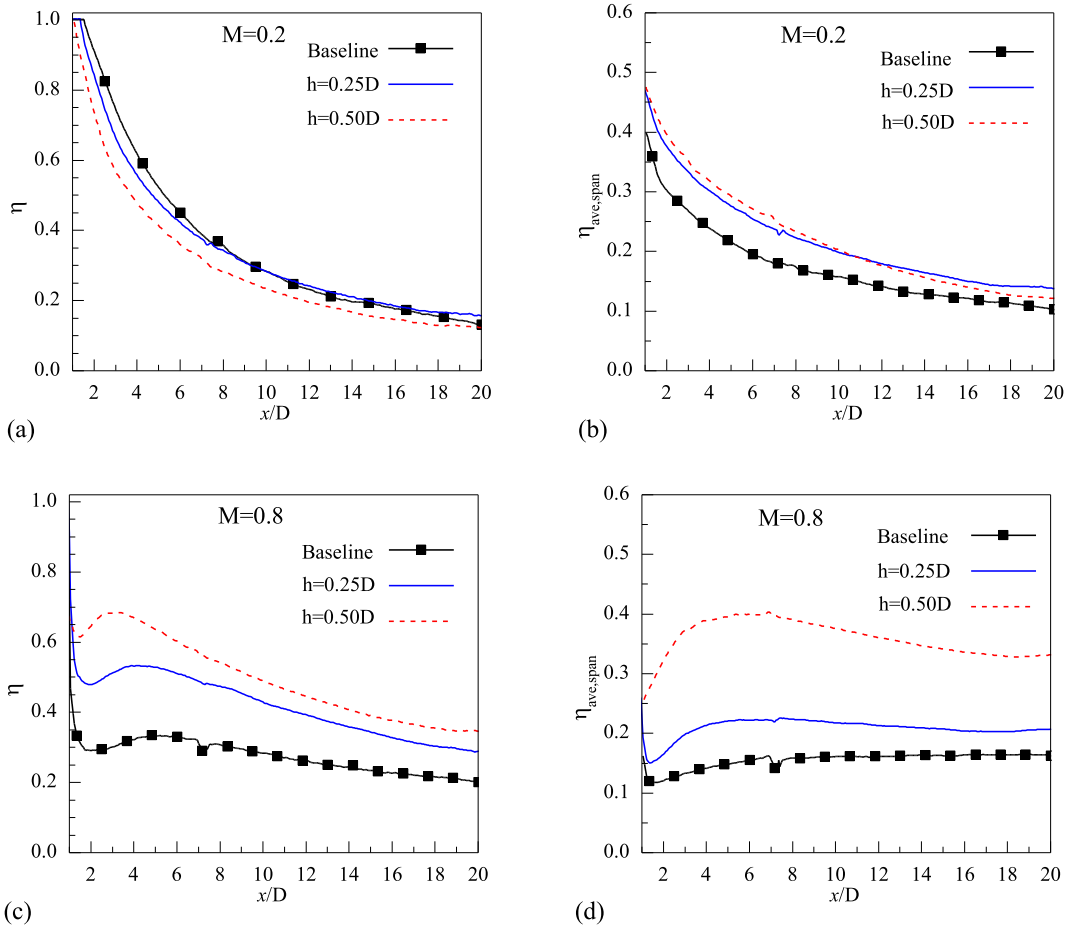

Fig. 14. Film cooling effectiveness for different VG heights; (a) centerline film cooling effectiveness, M = 0.2; (b) spanwise-averaged film cooling effectiveness, M = 0.2; (c) centerline film cooling effectiveness, M = 0.8; (d) spanwise-averaged film cooling effectiveness, M = 0.8.

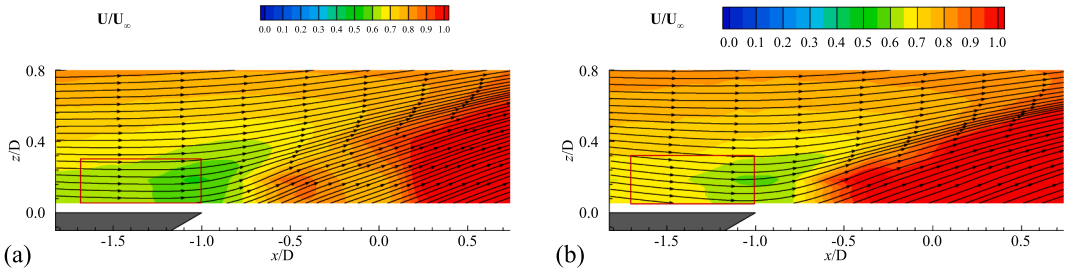

Fig. 15. Flow fields measured in the streamwise plane with different VG heights at M = 0.8 (a) h = 0.25D; (b) h = 0.5D.

Therefore, the streamwise location of the VG should be optimized carefully when the blowing ratio has a wide range.

The dimensional analysis of film cooling problem was systemically conducted by Baldauf and Scheurlen [32]. They indicated that the dimensionless parameters of influence on the film cooling effectiveness can be given as:

$$\eta = f\left(Re_D, Ec, Tu, I, M, \frac{x}{D}, \frac{y}{D}, \beta, \frac{s}{D}, \frac{l}{D}, \frac{\delta_1}{D}\right) \tag{4}$$

where Ec and Tu are the Eckert number and the turbulence intensity of the main flow, respectively. I is the momentum flux ratio of mainstream to coolant flow, and δ_1 is the displacement thickness of the boundary layer just upstream of the injection hole without coolant gas.

The main difference between the present study and Baldauf and Scheurlen [32] is the introduction of VG structure. Thus, the geometry parameters of VG, namely the height, width, length of the VG and the distance between the VG and the downstream film cooling hole, should be taken into consideration in the dimensional analysis.

$$h, w, l_{VG}, L \tag{5}$$

Therefore, the dimensionless parameters for the film cooling effectiveness can be shown as:

$$\eta = f\left(Re_D, Ec, Tu, I, M, \frac{x}{D}, \frac{y}{D}, \beta, \frac{s}{D}, \frac{l}{D}, \frac{\delta_1}{D}, \frac{h}{D}, \frac{w}{D}, \frac{l_{VG}}{D}, \frac{L}{D}\right) \tag{6}$$

In the present study, six dimensionless parameters (i.e., I,M,x/D,y/D, h/D, L/D) were varied to explore their influences on the film cooling performance over a VG structured film cooling surface. It can be found that the upstream VG structure can significantly enhance the film cooling effectiveness at relatively high blowing ratio. This is mainly

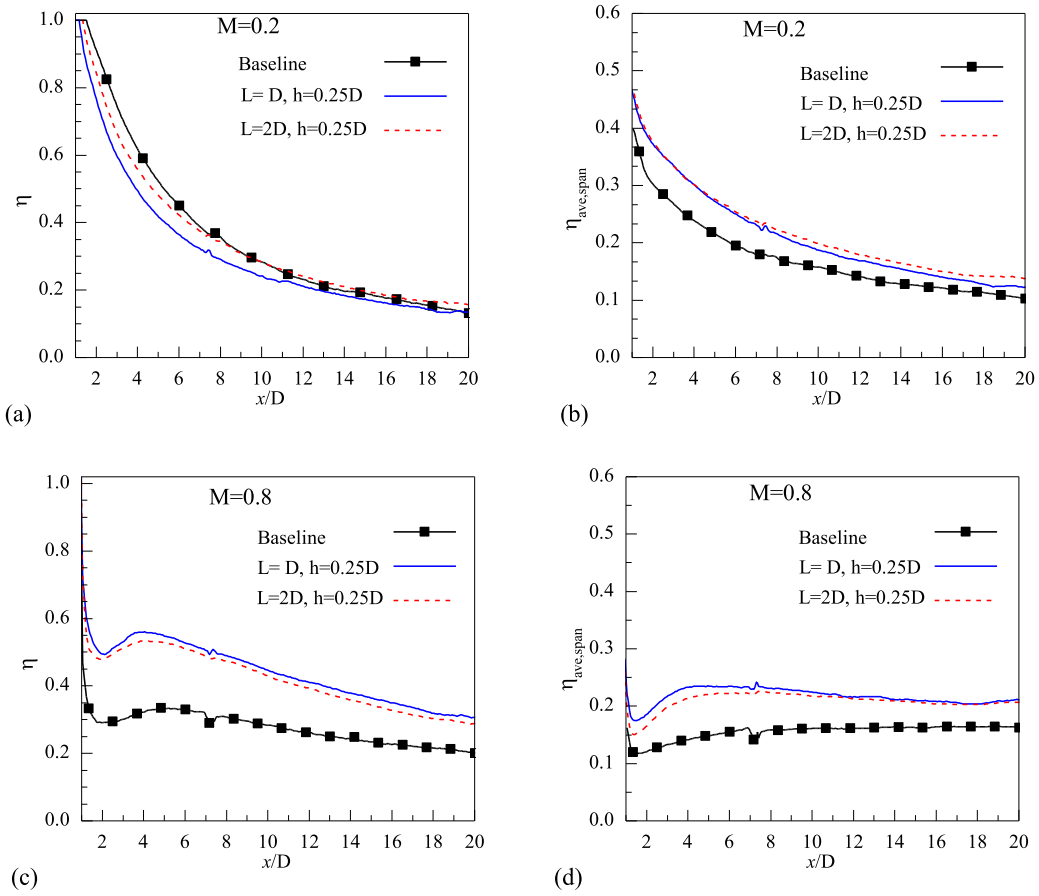

Fig. 16. Film cooling effectiveness profiles for different VG locations; (a) centerline film cooling effectiveness, M = 0.2; (b) spanwise-averaged film cooling effectiveness, M = 0.2; (c) centerline film cooling effectiveness, M = 0.8; (d) spanwise-averaged film cooling effectiveness, M = 0.8.

related to the anti-CRVP and downwash flow generated by the VG, which retard the separation of coolant gas from the surface of interest. In addition, while the film cooling effectiveness can be significantly influenced by the VG height (h/D), the streamwise location of VG (L/D) was found to has much less impact on the film cooling performance.

As described above, the present study demonstrated that the proposed upstream VG concept can be used to improve the film cooling effectiveness. However, more extensive studies are still needed to elucidate the associated underlying physics and systemically examine the relevant dimensionless parameters shown in Eq. (6), in order to explore/optimize design paradigms for better film cooling protection of turbine blades from harsh environments.

4. Conclusion

An experimental study was performed to evaluate the effects of an upstream micro VG on the film cooling performance as coolant gas was injected from downstream circular holes. A PSP technique based on the analogy of heat and mass transfer was used instead of the traditional temperature-based methods for measuring the film cooling effectiveness. In addition, a high-resolution PIV system was employed to explore the evolution of the flow structures downstream of the cooling hole in the streamwise plane and cross-plane. The relationship between the film cooling effectiveness and the flow field measurements was determined to elucidate the underlying mechanisms responsible for the improvements in the film cooling performance by the upstream micro VG structure.

The PSP measurement results revealed that the film cooling effectiveness on the test surface was improved significantly by the VG mounted upstream of the cooling hole within the range of blowing ratios investigated in this study. This effect was more pronounced at relatively high blowing ratios (M = 0.4 and 0.8). The cooling film coverage in the spanwise direction on the test surface was much more uniform than that of the baseline case. The spanwise-averaged film cooling effectiveness at the blowing ratio of M = 0.8 was 56–188% higher than that of the baseline case.

The flow characteristics obtained from the PIV measurements indicated that the dominant flow structure downstream of the cooling hole consisted of two pairs of large-scale counter-rotating vortices. One was generated by the injection of the coolant jet and was referred to as the CRVP. This CRVP in the coolant jet promotes the entrainment of the coolant gas into the main flow and entrains the mainstream to the surface in the outer region of the jet, resulting in a decrease in the film cooling performance. Another CRVP, whose rotation direction was opposite to that of the CRVP, was generated by the VG. This vortex pair was referred to as the anti-CRVP, which pushed the lifted coolant jet toward the surface, thereby improving the film cooling performance. Meanwhile, the anti-CRVP increased the coverage area of the coolant gas due to its rotation direction, resulting in a more uniform distribution of the film cooling effectiveness in the spanwise direction.

CRediT authorship contribution statement

Kuan Zheng: Formal analysis, Writing - original draft. **Wei Tian:** Conceptualization, Methodology, Formal analysis, Writing - review & editing, Funding acquisition, Supervision. **Jiang Qin:** Methodology, Formal analysis. **Hui Hu:** Conceptualization, Formal analysis, Writing - review & editing, Supervision.

Declaration of Competing Interest

The authors declare that they have no known competing financial interests or personal relationships that could have appeared to influence the work reported in this paper.

Acknowledgement

Funding support from National Natural Science Foundation of China (No. 11872039) is gratefully acknowledged.

References

[1] J.C. Han, S. Dutta, S. Ekkad, Gas Turbine Heat Transfer and Cooling Technology, CRC Press, Boca Raton, 2013.
[2] D.G. Bogard, K.A. Thole, Gas turbine film cooling, J. Propul. Power 22 (2) (2006) 249–270.
[3] E. Sakai, T. Takahashi, H. Watanabe, Large-eddy simulation of an inclined round jet issuing into a crossflow, Int. J. Heat Mass Transf. 69 (2014) 300–311.
[4] C. Dai, L. Jia, J. Zhang, Z. Shu, J. Mi, On the flow structure of an inclined jet in crossflow at low velocity ratios, Int. J. Heat Fluid Flow 58 (2016) 11–18.
[5] R.M. Kelso, T.T. Lim, A.E. Perry, An experimental study of round jets in cross-flow, J. Fluid Mech. 306 (1996) 111.
[6] B.A. Haven, M. Kurosaka, Kidney and anti-kidney vortices in crossflow jets, J. Fluid Mech. 352 (1997) 27–64.
[7] T.H. New, T.T. Lim, S.C. Luo, Elliptic jets in cross-flow, J. Fluid Mech. 494 (10) (2003) 119–140.
[8] A. Sau, T.W. Sheu, S.F. Tsai, R.R. Hwang, T.P. Chiang, Structural development of vortical flows around a square jet in cross-flow, in: Proceedings of the Royal Society of London. Series A: Mathematical, Physical and Engineering Sciences, 460 (2051) (2004) 3339-3368.
[9] K. Mahesh, The interaction of jets with crossflow, Annu. Rev. Fluid Mech. 45 (2013) 379–407.
[10] R.J. Goldstein, E.R.G. Eckert, F. Burggraf, Effects of hole geometry and density on three-dimensional film cooling, Int. J. Heat Mass Transf. 17 (5) (1974) 595–607.
[11] R.S. Bunker, A review of shaped hole turbine film-cooling technology, J. Heat Transf. 127 (4) (2005) 441–453.
[12] B.A. Haven, D.K. Yamagata, M. Kurosaka, S. Yamawaki, T. Maya, Anti-kidney pair of vortices in shaped holes and their influence on film cooling effectiveness, in: Proceedings of the ASME 1997 International Gas Turbine and Aeroengine Congress and Exhibition, Paper No. 97-GT-045 (1997) V003T009A007.
[13] J.E. Sargison, S.M. Guo, M.L.G. Oldfield, G.D. Lock, A.J. Rawlinson, A converging slot-hole film-cooling geometry-part 1: low-speed flat-plate heat transfer and loss, J. Turbomach. 124 (3) (2002) 461–471.
[14] J.E. Sargison, S.M. Guo, M.L.G. Oldfield, G.D. Lock, A.J. Rawlinson, A converging slot-hole film-cooling geometry-part 2: transonic nozzle guide vane heat transfer and loss, J. Turbomach. 124 (3) (2002) 453–460.
[15] T.F. Fric, R. P. Campbell, Method for improving the cooling effectiveness of a gaseous coolant stream which flows through a substrate, and related articles of manufacture, US. Patent No 6383602 B1, US, 2002.
[16] R.S. Bunker, Film cooling effectiveness due to discrete holes within a transverse surface slot, in: Proc. ASME Turbo Expo, Paper No. GT2002-30178 (2002) 129-138.
[17] D.T. Vogel, Numerical investigation of the influence of specific vortex generation on the mixing process of film cooling jets, in: Proc. ASME International Gas Turbine and Aeroengine Congress and Exhibition, Paper No. 98-GT-210 (1998) V004T09A051.
[18] K. Kusterer, D. Bohn, T. Sugimoto, R. Tanaka, Double-jet ejection of cooling air for improved film cooling, J. Turbomach. 129 (4) (2007) 809–815.
[19] K. Kusterer, A. Elyas, D. Bohn, T. Sugimoto, R. Tanaka, M. Kazari, The NEKOMIMI cooling technology: cooling holes with ears for high-efficient film cooling, in: Proc. ASME Turbo Expo, Paper No. GT2011-45524 (2011) 303-313.
[20] J.D. Heidmann, S. Ekkad, A novel antivortex turbine film-cooling hole concept, J. Turbomach. 130 (3) (2008), 031020.
[21] M.J. Ely, B.A. Jubran, A numerical study on improving large angle film cooling performance through the use of sister holes, Numer. Heat Tranf. A-Appl. 55 (7) (2009) 634–653.
[22] M.J. Ely, B.A. Jubran, A numerical evaluation on the effect of sister holes on film cooling effectiveness and the surrounding flow field, Heat Mass Transf. 45 (11) (2009) 1435–1446.
[23] Y. Lu, A. Dhungel, S.V. Ekkad, R.S. Bunker, Effect of trench width and depth on film cooling from cylindrical holes embedded in trenches, J. Turbomach. 131 (1) (2009), 011003.
[24] S. Na, T.I. Shih, Increasing adiabatic film-cooling effectiveness by using an upstream ramp, J. Heat Transf. 129 (4) (2007) 464–471.
[25] D.L. Rigby, J.D. Heidmann, Improved film cooling effectiveness by placing a vortex generator downstream of each hole, in: Proc. ASME Turbo Expo, Paper No. GT2008-51361 (2008) 1161-1174.
[26] K.B. Zaman, D.L. Rigby, J.D. Heidmann, Inclined jet in crossflow interacting with a vortex generator, J. Propul. Power 26 (2010) 947–954.
[27] K.B. Zaman, D.L. Rigby, J.D. Heidmann, Experimental study of an inclined jet-in-cross-flow interacting with a vortex generator, in: 48th AIAA Aerospace Sciences Meeting Including the New Horizons Forum and Aerospace Exposition, Paper No. AIAA 2010-88, 2010.
[28] A.F. Shinn, S.P. Vanka, Large eddy simulations of film-cooling flows with a micro-ramp vortex generator, J. Turbomach. 135 (1) (2012), 011004.
[29] L. Song, C. Zhang, Y. Song, J. Li, Z. Feng, Experimental investigations on the effects of inclination angle and blowing ratio on the flat-plate film cooling enhancement using the vortex generator downstream, Appl. Therm. Eng. 119 (2017) 573–584.
[30] A. Suryanarayanan, S.P. Mhetras, M.T. Schobeiri, J.C. Han, Film-cooling effectiveness on a rotating blade platform, J. Turbomach. 131 (1) (2009), 011014.
[31] Z. Yang, H. Hu, Trailing edge cooling effectiveness measurements of turbine blades using pressure sensitive paint (PSP) technique, J. Propul. Power 27 (3) (2011) 700–709.
[32] S. Baldauf, M. Scheurlen, CFD based sensitivity study of flow parameters for engine like film cooling conditions, in: ASME 1996 International Gas Turbine and Aeroengine Congress and Exhibition, Paper No. 96-GT-310, 1996.
[33] J.B. Anderson, E.K. Wilkes, J.W. McClintic, D.G. Bogard, Effects of freestream Mach number, Reynolds number, and boundary layer thickness on film cooling effectiveness of shaped holes, in: ASME Turbo Expo 2016: Turbomachinery Technical Conference and Exposition, 2016.
[34] J.N. Shadid, E.R.G. Eckert, The mass transfer analogy to heat transfer in fluids with temperature-dependent properties, J. Turbomach. 113 (1) (1991) 27–33.
[35] W. Zhou, H. Hu, Improvements of film cooling effectiveness by using barchan dune shaped ramps, Int. J. Heat Mass Transf. 103 (2016) 443–456.
[36] B. Johnson, B., W. Tian, K. Zhang, H. Hu, An experimental study of density ratio effects on the film cooling injection from discrete holes by using PIV and PSP techniques, Int. J. Heat Mass Transf. 76 (2014), 337–349.
[37] D. Charbonnier, P. Ott, M. Jonsson, F. Cottier, T. Kobke, Experimental and Numerical Study of the Thermal Performance of a Film Cooled Turbine Platform, in: ASME Turbo Expo 2009: Power for Land, Sea, and Air, Paper NO. GT2009-60306, 2009.
[38] B. Johnson, H. Hu, Measurement uncertainty analysis in determining adiabatic film cooling effectiveness by using pressure sensitive paint technique, J. Turbomach. 138 (12) (2016), 121004.
[39] M. Raffel, C.E. Willert, S.T. Wereley, J. Kompenhans, Particle image velocimetry: a practical guide, 2nd edn., Springer, Berlin, 2007.
[40] M.S. Chong, A.E. Perry, B.J. Cantwell, A general classification of three-dimensional flow fields, Phys. Fluids 2 (5) (1990) 765–777.